Nanoscale

PAPER

View Article Online
View Journal | View Issue

Cite this: *Nanoscale*, 2018, **10**, 15564

Graphene-based dual-band independently tunable infrared absorber

Peng Sun,[a,b] Chenglong You,[c] Amirreza Mahigir,[d,e] Tongtong Liu,[a,b] Feng Xia,[a,b] Weijin Kong,[a,b] Georgios Veronis,[d,e] Jonathan P. Dowling,[c,f] Lifeng Dong[g,h] and Maojin Yun *[a,b]

Received 28th March 2018,
Accepted 31st July 2018

DOI: 10.1039/c8nr02525h

rsc.li/nanoscale

In this paper, we theoretically demonstrate a dual-band independently tunable absorber consisting of a stacked graphene nanodisk and graphene layer with nanohole structure, and a metal reflector spaced by insulator layers. This structure exhibits a dipole resonance mode in graphene nanodisks and a quadrupole resonance mode in the graphene layer with nanoholes, which results in the enhancement of absorption over a wide range of incident angles for both TE and TM polarizations. The peak absorption wavelength is analyzed in detail for different geometrical parameters and the Fermi energy levels of graphene. The results show that both peaks of the absorber can be tuned dynamically and simultaneously by varying the Fermi energy level of graphene nanodisks and graphene layer with nanoholes structure. In addition, one can also independently tune each resonant frequency by only changing the Fermi energy level of one graphene layer. Such a device could be used as a chemical sensor, detector or multi-band absorber.

1 Introduction

Surface plasmon-polaritons (SPPs) are excitations of electromagnetic radiation coupled to surface charges existing at a metal–dielectric interface, which propagate along the interface.[1,2] When this occurs in metallic nanoparticles, the corresponding non-propagating plasmon-polaritons are generally denoted as localized surface plasmons (LSPs).[3–5]

Similar to a three-dimensional (3D) metal nanoparticle, a doped two-dimensional (2D) graphene monolayer can also support SPPs.[6–13] Graphene, a two-dimensional material of hexagonally arranged carbon atoms, has attracted significant attention for its remarkable properties such as electrical tunability, strong light confinement, and relatively low ohmic losses.[14] In virtue of the tunability of its carrier mobility and conductivity, countless studies focus on perfect absorbers based on graphene. Tunable metamaterial absorbers based on graphene have been widely investigated.[15–19] However, in these studies only single band absorption was reported. Dual-band or multi-band tunable perfect absorbers were also presented based on graphene elliptical nanodisk and multilayered graphene structures.[20–22] However, in these structures, different absorption bands cannot be controlled or tuned independently from each other. In addition, multiband metamaterial absorbers based on combining two cross-shaped metallic resonators of different sizes that can independently tune absorption bands have been reported.[23]

In this paper, different from traditional optical absorbers based on a single graphene layer,[15–19,21,23] we design an independently tunable dual-band absorber by double-stacked graphene layers, which does not require fabrication of metallic nanostructures. The absorption can be significantly enhanced due to the dipole and quadrupole resonance modes, which are supported by graphene nanodisks and graphene layer with nanoholes, respectively. The effect of geometrical parameters on the absorption spectra is studied. A wide spectral range of absorption wavelengths can be realized by changing the geometrical parameters of the structure. Moreover, the main advantage is that our proposed structure possesses excellent properties of flexible selective spectral absorption in a wide spectral range by slightly changing only the Fermi energy level of one of the graphene layers. Besides, the absorption remains more than 90% over a wide range of incident angles for both TE and TM polarizations. This tunable structure could be

[a]College of Physics Science, Qingdao University, Qingdao 266071, China. E-mail: mjyun@qdu.edu.cn
[b]Key Laboratory of Photonics Materials and Technology in Universities of Shandong, Qingdao University, Qingdao 266071, China
[c]Hearne Institute for Theoretical Physics and Department of Physics and Astronomy, Louisiana State University, Baton Rouge, Louisiana 70803, USA
[d]School of Electrical Engineering and Computer Science, Louisiana State University, Baton Rouge, Louisiana 70803, USA
[e]Center for Computation and Technology, Louisiana State University, Baton Rouge, Louisiana 70803, USA
[f]NYU-ECNU Institute of Physics at NYU Shanghai, 3663 Zhongshan Road North, Shanghai, 200062, China
[g]School of Chemistry and Pharmaceutical Engineering, Taishan Medical University, Taian 271016, China
[h]Department of Physics, Hamline University, Saint Paul, MN 55104, USA

useful for applications related to chemical sensors, detectors, and multi-band absorbers.

2 Results

The schematic of the proposed infrared absorber is shown in Fig. 1. Arrays of doped single-layer graphene nanodisks with diameter D_1 = 175 nm and nanoholes with diameter D_2 = 385 nm are placed on the top surface of two insulator layers. The optically thick gold layer which is used as the back reflector prevents any transmission through the structure. In this way, the transmission from this structure is inhibited and perfect absorption can be obtained when the reflection is close to zero.[24] Also note that the two graphene layers are concentric in the z direction. The thickness of the two insulators are s_1 = 60 nm and s_2 = 1.7 μm. The structure is periodic in the x and the y directions with periodicity P = 400 nm. The structure is illuminated by a normally-incident monochromatic plane wave with electric field along the x direction.

The relative dielectric permittivity of the insulator which is assumed to be lossless is 1.96.[25] The permittivity of gold is calculated using the Drude model with plasma frequency ω_p = 1.37×10^{16} s^{-1} and damping constant ω_τ = 1.23×10^{14} s^{-1}.[25] All materials are considered as nonmagnetic (μ_r = 1).

Graphene is modeled in the simulations as a conductive surface with thickness t_g = 1 nm.[26] The surface conductivity of graphene is expressed by the Kubo formula within the local random phase approximation including interband and intraband transitions[27–29]

$$\sigma_\omega = \frac{2e^2 k_B T}{\pi\hbar^2}\frac{i}{\omega + i\tau^{-1}}\ln\left[2\cosh\left(\frac{E_F}{2k_B T}\right)\right] + \frac{e^2}{4\hbar}\left[\frac{1}{2} + \frac{1}{\pi}\arctan\left(\frac{\hbar\omega - 2E_F}{2k_B T}\right)\right] - \frac{e^2}{4\hbar}\left[\frac{i}{2\pi}\ln\frac{(\hbar\omega + 2E_F)^2}{(\hbar\omega - 2E_F)^2 + 4(k_B T)^2}\right], \quad (1)$$

where e is the electron charge, k_B is the Boltzmann constant, T is the temperature, $\hbar$ is the reduced Planck's constant, E_F is the Fermi energy level, ω is the photon frequency in vacuum, and $\tau = \mu E_F/(e\nu_F^2)$ stands for the momentum relaxation time due to charge carrier scattering. Here we use the Fermi velocity $\nu_F = 1 \times 10^6$ m s^{-1} and dc mobility μ = 10 000 cm^2 V^{-1} s^{-1}.[30] When the Fermi level is increased above half of the photon energy, the interband contribution of graphene conductivity is very small according to the Pauli exclusion principle.[25] In our simulations, we only consider highly doped graphene with the Fermi energy level $E_F \gg k_B T$ and $E_F \gg \hbar\omega$, so the conductivity of graphene can be simplified as:[8,31]

$$\sigma_\omega = \frac{e^2 E_F}{\pi\hbar^2}\frac{i}{\omega + i\tau^{-1}}. \quad (2)$$

E_F is determined by the doping concentration. In practical operation, although the graphene nanodisks are not electrically interconnected, their Fermi energy levels can be tuned through a thin layer of gel-like ion liquid which is placed on top of the sample and acts as a conductive contact.[32,33] The use of ion gels for creating conductive contacts has been described in detail elsewhere.[34] Here we assume that the same approach as the one described in ref. 34 is used, and that the entire uppermost surface of the sample, where the nanodisks are located, is covered with the ion gel. This enables us to tune the Fermi energy level of the nanodisks. A gate voltage can be applied between the conductive contact and the gold reflector. The Fermi energy of the graphene layer with nanoholes can be tuned *via* electrostatic biasing by applying a gate voltage between the gold reflector and the graphene layer. In this work, numerical simulations were carried out based on the finite element method (FEM). The transmission $T(\omega)$ is zero in our structure since the gold film thickness is assumed to be infinite. Thus the absorption is given by $A(\omega) = 1 - R(\omega)$, where $R(\omega)$ is the reflection.

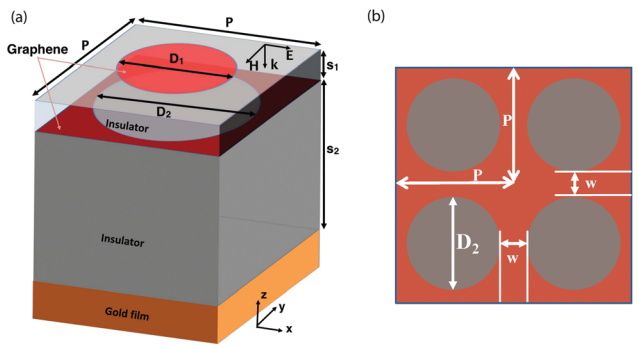

Fig. 1 (a) Schematic of a unit cell of the proposed graphene-based infrared absorber. (b) Schematic of the graphene layer with an array of nanoholes.

3 Discussion

Fig. 2 shows the absorption spectra of the structure (black solid line). For comparison, the absorption spectra for the structure without nanoholes (red dashed line) and without nanodisks (blue dashed line) are also plotted. Graphene Fermi energies were chosen as E_F^D = 0.5 eV and E_F^H = 0.65 eV for the nanodisks and the layer with nanoholes, respectively. The spectra show that two absorption peaks, denoted as A and B, occur in the proposed structure, which are contributed by the graphene nanodisks and the graphene layer with nanoholes, respectively. The resonance wavelengths corresponding to the two absorption peaks are λ_A = 11.92 μm and λ_B = 14.55 μm, respectively. Keeping other parameters fixed, the red (blue) dashed line in Fig. 2 corresponds to the absorption spectra of the proposed structure without the lower (upper) graphene layer. Through the comparison of the solid and dashed lines, we find that the overall absorption spectra are approximately the combination of structures with only an array of graphene nanodisks or a graphene layer with an array of nanoholes.

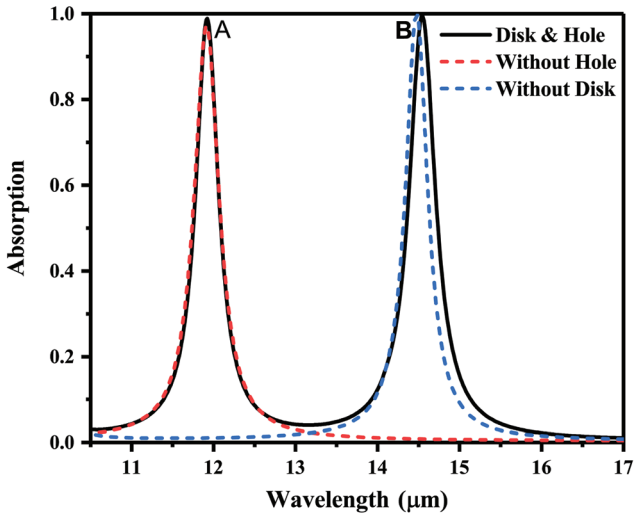

Fig. 2 Absorption spectra for the structure shown in Fig. 1 (black solid line). Also shown are the absorption spectra of the structure shown in Fig. 1 without the graphene layer with an array of nanoholes (red dashed line), and the spectra of the structure without the array of graphene nanodisks (blue dashed line). All parameters are as in Fig. 1.

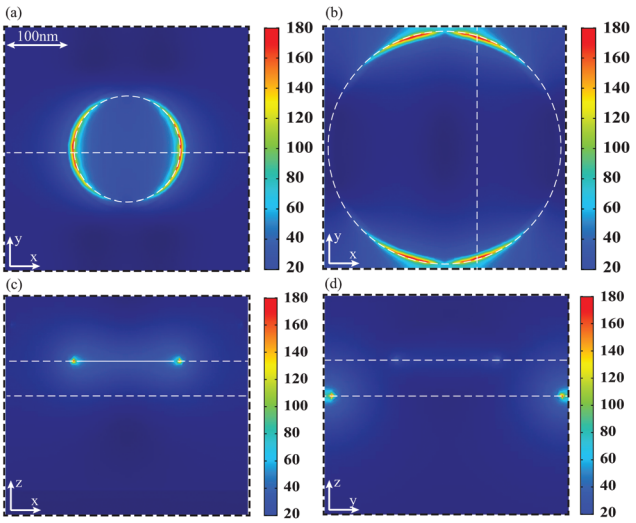

Fig. 3 (a) Profile of the electric field amplitude normalized by the field amplitude of the incident plane wave at the plane of the array of graphene nanodisks. Results are shown at the wavelength corresponding to absorption peak A in Fig. 2. All other parameters are as in Fig. 1. (b) Profile of the electric field amplitude normalized by the field amplitude of the incident plane wave at the plane of the graphene layer with an array of nanoholes. Results are shown at the wavelength corresponding to absorption peak B in Fig. 2. All other parameters are as in Fig. 1. (c) Profile of the electric field amplitude normalized by the field amplitude of the incident plane wave at the x–z plane shown with dashed line in (a). Results are shown at the wavelength corresponding to absorption peak A in Fig. 2. All other parameters are as in Fig. 1. (d) Profile of the electric field amplitude normalized by the field amplitude of the incident plane wave at the y–z plane shown with dashed line in (b). Results are shown at the wavelength corresponding to absorption peak B in Fig. 2. All other parameters are as in Fig. 1.

In order to understand the physical origin of the two absorption peaks, we consider the normalized electric field amplitude corresponding to absorption peaks A and B. From Fig. 3(a) and (c), we observe that a dipole resonance mode is supported by the graphene nanodisks. The electric field of this mode is highly localized in the graphene nanodisks, while the electric field intensity at the graphene layer with nanoholes is almost zero. Thus, at the resonance wavelength A (Fig. 2) light is absorbed at the graphene nanodisks. Similarly, from Fig. 3(b) and (d), we observe that a quadrupole resonance mode is supported by the graphene layer with nanoholes in the lower graphene layer. The electric field of this mode is highly localized in the graphene layer with nanoholes, while the electric field intensity at the graphene nanodisks is almost zero. Thus, at the resonance wavelength B (Fig. 2) light is absorbed at the graphene layer with nanoholes. These analyses prove that there is almost no coupling effect between the two graphene layers. Therefore, the two absorption peaks can be independently tuned by varying the Fermi energy level of the graphene nanodisks and the graphene layer with nanoholes.

Perfect absorption can be achieved when the effective impedance of the structure matches that of free space, resulting in zero reflection. Therefore, the thickness s_2 of the insulator layer directly impacts the absorption of the structure. Fig. 4 shows the absorption spectra as a function of the thickness s_2 of the insulator layer. As shown in Fig. 4, varying s_2 has no significant effect on the position of the resonant peak, but greatly affects the total absorption in the structure. This is due to Fabry–Perot effects in the second insulator layer with thickness s_2. We choose s_2 = 1.7 μm. For this thickness, the effective impedance of the structure matches that of free space at the resonance wavelengths, so that the overall reflection from the sample vanishes. Thus, all of the incident power is absorbed in the structure.

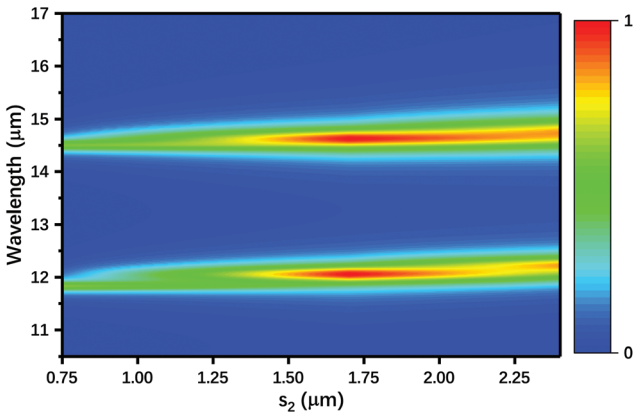

Fig. 4 Absorption spectra of the structure shown in Fig. 1 as a function of the thickness s_2 of the lower insulator layer. All other parameters are as in Fig. 1.

In addition, the effect of the other geometrical parameters (D_1, D_2, s_1, and P in Fig. 1) on the absorption spectra are investigated in Fig. 5(a)–(d). These analyses provide some guidance to structural design and fabrication.

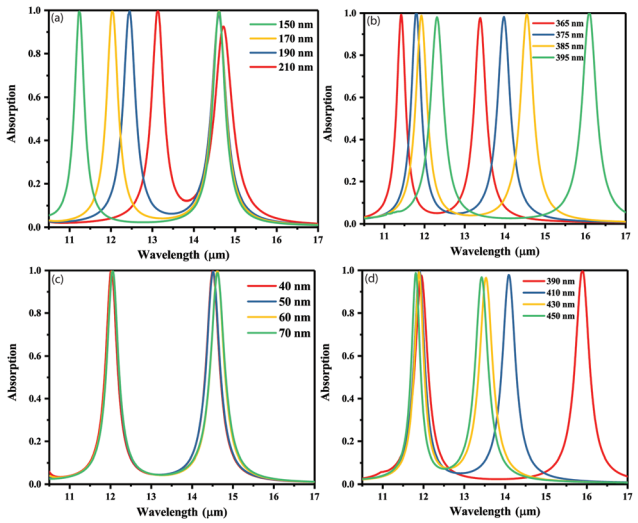

Fig. 5 (a) Absorption spectra of the structure shown in Fig. 1 as a function of the nanodisk diameter D_1. All other parameters are as in Fig. 1. (b) Absorption spectra of the structure shown in Fig. 1 as a function of the nanohole diameter D_2. All other parameters are as in Fig. 1. (c) Absorption spectra of the structure shown in Fig. 1 as a function of the thickness s_1 of the upper insulator layer. All other parameters are as in Fig. 1. (d) Absorption spectra of the structure shown in Fig. 1 as a function of the period of the structure P. All other parameters are as in Fig. 1.

The plasmon resonance of an individual graphene disk occurs at an energy[32,33]

$$\hbar\omega_p \approx \sqrt{\frac{2\alpha\hbar c L_1 E_F}{\pi(\varepsilon_1+\varepsilon_2)D}}, \quad (3)$$

and the corresponding resonant wavelength can be expressed as

$$\lambda_p \approx \sqrt{\frac{2\pi^3 c\hbar(\varepsilon_1+\varepsilon_2)D}{\alpha L_1 E_F}}, \quad (4)$$

where $\alpha \approx 1/137$ is the fine-structure constant, c is the speed of light in free space, L_1 is a constant which is independent of frequency and disk size but depends on the symmetry of the plasmon, ε_1 and ε_2 are the dielectric permittivities of the materials above and below the graphene disk, respectively, and D is the diameter of the graphene disk.

The evolution of the absorption spectra with varying nanodisk diameter D_1 and nanohole diameter D_2 with other parameters unaltered are illustrated in Fig. 5(a) and (b), respectively. We observe that the resonant wavelength of absorption peak A has a redshift from 11.23 μm to 13.14 μm as D_1 varies from 150 nm to 210 nm, and the position of absorption peak B is almost constant. The resonant wavelength of peak A increases when the disk diameter becomes larger, which can be understood from eqn (4). More specifically, we observe that the resonant wavelength is approximately proportional to $\sqrt{D}$, as expected from eqn (4). Meanwhile, the peak absorption remains high in a wide spectral range.

As can be observed from Fig. 5(b), absorption peak B shows a redshift from 13.38 μm to 16.11 μm as D_2 varies from 365 nm to 395 nm. This is similar to Fig. 5(a), resulting from the resonant wavelength increasing with D_2. However, unlike Fig. 5(a), the wavelength of absorption peak A changes when D_2 varies. This can be explained *via* the following analysis. The effective permittivity of the dielectric layer, below the graphene nanodisks, can be affected by changing D_2. In Fig. 3(b), the field is confined with high local intensity in a narrow graphene strip with a width much smaller than the period. In analogy to metallic slits,[35–37] the effective permittivity of thedielectric layer can be approximated as

$$\varepsilon_{eff} \approx \varepsilon P/w, \quad (5)$$

where ε is the dielectric constant of the insulator, P is the period, and w is the width of the graphene strip [shown in Fig. 1(b)]. The reference value of D_2 is 385 nm with an absorption peak A at 11.92 μm. The width of graphene strip w increases when D_2 varies from 385 nm to 365 nm, resulting in a decrease of ε_{eff}. As a result, based on eqn (4), the resonant wavelength of peak A shows a blueshift from 11.92 μm to 11.41 μm. Similarly, the resonant wavelength of peak A exhibits a redshift when we increase D_2 to 395 nm.

We choose the thickness of the top insulator s_1 = 60 nm, which is much smaller than the operation wavelength of the device, to prevent Fabry–Pérot effects associated with the top insulator layer. Therefore, when the absorption spectra are calculated for different thicknesses of the top insulator layer s_1, ranging from 40 nm to 70 nm, while other parameters are kept unchanged, no major change in the resonance wavelengths is observed [Fig. 5(c)].

The effect of changing the period P of the structure on the absorption spectra is shown in Fig. 5(d). As P increases from 390 nm to 450 nm, the absorption peak B is blueshifted from 15.90 μm to 13.43 μm due to the increase of L_1. For a standard graphene nanoring, L_1 increases with the decreasing of the ratio of inner to outer diameter.[32] Also, the absorption peak B exhibits a slight blueshift from 11.94 μm to 11.81 μm with the period varying from 390 nm to 450 nm. However, since P/w hardly changes when P increases with a fixed D_2, ε_{eff} hardly decreases. According to eqn (4), it can be seen that the resonance will occur at a shorter wavelength.

Fig. 6(a) [6(b)] shows the absorption spectra, under the condition that only the Fermi energy of the graphene nanodisks (graphene layer with nanoholes) varies, while the rest of the parameters are unchanged. As the Fermi energy of the graphene nanodisks (graphene layer with nanoholes) increases from 0.43 eV to 0.58 eV (0.50 eV to 0.70 eV), the resonance wavelength of peak A (B) experiences a blueshift and decreases from 12.82 μm to 11.08 μm (16.55 μm to 14.02 μm), a wavelength shift of 13.6% (15.3%), while the position of the other absorption peak does not change, which indicates that there is no coupling effect between the two graphene layers in process of graphene Fermi energy adjusting. Therefore, the absorption spectra can be independently tuned in a wide spectral range by

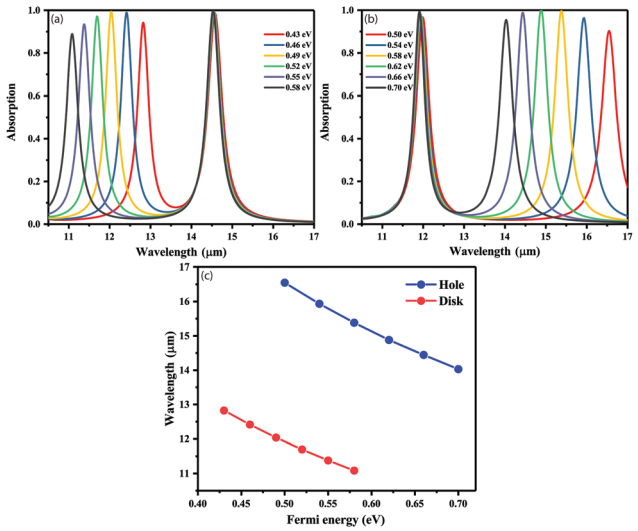

Fig. 6 (a) Absorption spectra of the structure shown in Fig. 1 as a function of the Fermi level of the graphene nanodisks. All other parameters are as in Fig. 1. (b) Absorption spectra of the structure shown in Fig. 1 as a function of the Fermi level of the graphene layer with an array of nanoholes. All other parameters are as in Fig. 1. (c) Resonance wavelength A (Fig. 2) as a function of the Fermi level of the graphene nanodisks (red line). Also shown is the resonance wavelength B (Fig. 2) as a function of the Fermi level of the graphene layer with an array of nanoholes (blue line). All other parameters are as in Fig. 1.

changing the Fermi energy level of graphene. Increasing E_F can lead to an increase of resonant frequency.[21] In other words, this results in a decrease in the resonant wavelength,[38,39] which is in agreement with eqn (4). It is also clearly observed that we no longer have near perfect absorption. The reason is that the perfect impedance matching condition between the graphene structure and free space cannot be satisfied as E_F increases. However, the peak absorption remains high in a wide spectral range. We also study the relation between the resonance wavelength and the Fermi energy, which is shown in Fig. 6(c). The relation between the resonance wavelength of graphene nanodisks and graphene layer with nanoholes and the Fermi energy is shown with red and blue lines. Fig. 6(c) shows that the resonance wavelengths of graphene nanodisks and graphene layer with nanoholes are almost linearly proportional to the Fermi energy. Therefore, in our proposed structure, the resonance wavelengths of graphene nanodisks and graphene layer with nanoholes can be actively tuned by slightly changing the Fermi energy of graphene. This tunability feature of graphene-based structures makes them more attractive than metal-based devices in which the optical responses cannot be efficiently tuned.

In the preceding discussions, absorption spectra were shown for normally illuminated structures. Finally, the absorption spectra at different incident angles for TE and TM polarizations are illustrated in Fig. 7(a) and (b), respectively. Clearly, the absorption peaks are not sensitive to the angle of incidence, which can be attributed to the high degree of symmetry of the structure. In addition, we found that, since the resonances in the graphene nanodisks and graphene layer with nanoholes are localized, the resonance wavelengths are not sensitive to the incident angle.[25,40] Therefore, a peak absorption of ~90% is still achieved at incident angles as large as 65° for TE polarization and 50° for TM polarization. As the results reveal, the proposed structure is a wide-angle, polarization-independent absorber, which could be important for many practical applications.

4 Conclusion

In summary, we introduced graphene-based, dual-band, independently tunable infrared absorbers. The influence of various geometrical parameters on the absorption spectra of the structure were investigated in detail. Due to the dipole and quadru-

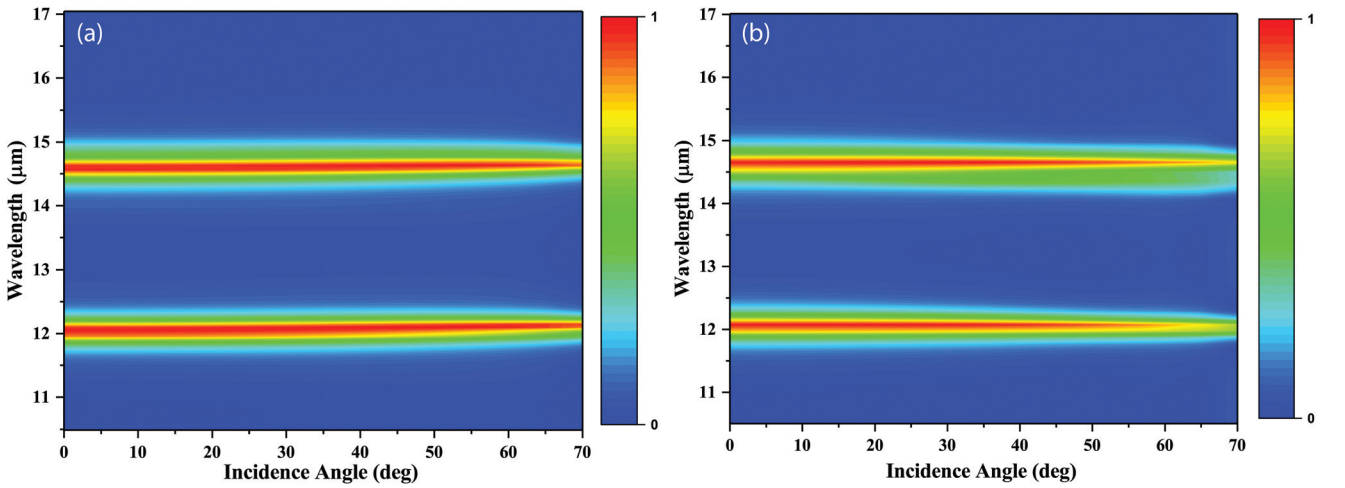

Fig. 7 (a) Absorption spectra of the structure shown in Fig. 1 as a function of the angle of incidence. Results are shown for TE polarization. All other parameters are as in Fig. 1. (b) Absorption spectra of the structure shown in Fig. 1 as a function of the angle of incidence. Results are shown for TM polarization. All other parameters are as in Fig. 1.

pole resonance modes, which are supported by an array of graphene nanodisks and a graphene layer with an array nanoholes, respectively, the absorption can be significantly enhanced. We found that the two absorption peaks of the structure can be independently tuned by varying the Fermi energy level of the graphene nanodisks and of the graphene layer with nanoholes. In addition, we found that the proposed structure is a wide-angle polarization-independent absorber. The proposed structure could be useful for applications related to chemical sensors, detectors, and multi-band infrared absorbers.

Conflicts of interest

There are no conflicts to declare.

Acknowledgements

This work is supported by the National Natural Science Foundation of China (51472174, 11144007, 11274188), Natural Science Foundation of Shandong Province under Grant ZR2017MF059, Optoelectronics Think Tank Foundation of Qingdao. C. Y. would like to acknowledge support from an Economic Development Assistantship from the Louisiana State University System Board of Regents. G. V. acknowledges financial support by National Science Foundation (NSF) (1254934). L. F. Dong acknowledges financial support by the Malmstrom Endowment Fund.

References

1 D. R. Tilley, *Opt. Acta: Int. J. Opt.*, 1983, **30**, 1501–1501.
2 J. Zhang, L. Zhang and W. Xu, *J. Phys. D: Appl. Phys.*, 2012, **45**, 113001.
3 M. Pelton, J. Aizpurua and G. Bryant, *Laser Photonics Rev.*, 2008, **2**, 136–159.
4 M. Pelton and G. Bryant, *Introduction to Metal-Nanoparticle Plasmonics*, John Wiley & Sons, New Jersey, 2013.
5 M. I. Stockman, *Phys. Today*, 2011, **64**, 39–44.
6 Y. V. Bludov, A. Ferreira, N. M. R. Peres and M. I. Vasilevskiy, *Int. J. Mod. Phys. B*, 2013, **27**, 1341001.
7 J. Christensen, A. Manjavacas, S. Thongrattanasiri, F. H. L. Koppens and F. Javier García de Abajo, *ACS Nano*, 2012, **6**, 431–440.
8 M. Jablan, H. Buljan and M. Soljačić, *Phys. Rev. B: Condens. Matter Mater. Phys.*, 2009, **80**, 245435.
9 M. Jablan, M. Soljačić and H. Buljan, *Proc. IEEE*, 2013, **101**, 1689–1704.
10 L. Ju, B. Geng, J. Horng, C. Girit, M. Martin, Z. Hao, H. A. Bechtel, X. Liang, A. Zettl, Y. R. Shen and F. Wang, *Nat. Nanotechnol.*, 2011, **6**, 630–634.
11 J. H. Strait, P. Nene, W. Chan, C. Manolatou, S. Tiwari, F. Rana, J. W. Kevek and P. L. McEuen, *Phys. Rev. B: Condens. Matter Mater. Phys.*, 2013, **87**, 291–295.
12 H. Yan, T. Low, W. Zhu, Y. Wu, M. Freitag, X. Li, F. Guinea, P. Avouris and F. Xia, *Nat. Photonics*, 2013, **7**, 394–399.
13 F. J. García de Abajo, *ACS Photonics*, 2014, **1**, 135–152.
14 X. Luo, T. Qiu, W. Lu and Z. Ni, *Mater. Sci. Eng., R*, 2013, **74**, 351–376.
15 S. Song, Q. Chen, L. Jin and F. Sun, *Nanoscale*, 2013, **5**, 9615–9619.
16 R. Alaee, M. Farhat, C. Rockstuhl and F. Lederer, *Opt. Express*, 2012, **20**, 28017–28024.
17 L. Li, M. Cao, T. Li, L. Meng, H. Zhang and Y. Zhang, *Mater. Res. Express*, 2017, **10**, 105801.
18 Y. Zhang, Y. Li, Y. Cao, Y. Liu and H. Zhang, *Opt. Commun.*, 2017, **382**, 281–287.
19 Y. Zhang, T. Li, H. Lv, X. Huang, X. Zhang, S. Xu and H. Zhang, *Chin. Phys. Lett.*, 2015, **32**, 169–172.
20 Z. Su, J. Yin and X. Zhao, *Opt. Express*, 2015, **23**, 1679–1690.
21 G. Yao, F. Ling, J. Yue, C. Luo, J. Ji and J. Yao, *Opt. Express*, 2016, **24**, 1518–1527.
22 M. Amin, M. Farhat and H. Bağcl, *Opt. Express*, 2013, **21**, 29938–29948.
23 Y. Zhang, T. Li, Q. Chen, H. Zhang, J. F. O'Hara, E. Abele, A. J. Taylor, H. Chen and A. K. Azad, *Sci. Rep.*, 2015, **5**, 18463.
24 J. R. Piper and S. Fan, *ACS Photonics*, 2014, **1**, 347–353.
25 J. Zhang, Z. Zhu, W. Liu, X. Yuan and S. Qin, *Nanoscale*, 2015, **7**, 13530–13536.
26 S. Thongrattanasiri, F. H. L. Koppens and F. J. García de Abajo, *Phys. Rev. Lett.*, 2012, **108**, 047401.
27 Q. Bao, H. Zhang, B. Wang, Z. Ni, C. H. Y. X. Lim, Y. Wang, D. Y. Tang and K. P. Loh, *Nat. Photonics*, 2011, **5**, 411–415.
28 G. W. Hanson, *J. Appl. Phys.*, 2008, **103**, 064302.
29 K. Li, F. Xia, M. Wang, P. Sun, T. Liu, W. Hu, W. Kong, M. Yun and L. Dong, *Carbon*, 2017, **118**, 192–199.
30 K. S. Novoselov, A. K. Geim, S. V. Morozov, D. Jiang, Y. Zhang, S. V. Dubonos, I. V. Grigorieva and A. A. Firsov, *Science*, 2004, **306**, 666–669.
31 G. W. Hanson, *J. Appl. Phys.*, 2008, **104**, 084314.
32 Z. Fang, S. Thongrattanasiri, A. Schlather, Z. Liu, L. Ma, Y. Wang, P. M. Ajayan, P. Nordlander, N. J. Halas and F. J. García de Abajo, *ACS Nano*, 2013, **7**, 2388–2395.
33 Z. Fang, Y. Wang, A. E. Schlather, Z. Liu, P. M. Ajayan, F. J. García de Abajo, P. Nordlander, X. Zhu and N. J. Halas, *Nano Lett.*, 2014, **14**, 299–304.
34 C. F. Chen, C. H. Park, B. W. Boudouris, J. Horng, B. Geng, C. Girit, A. Zettl, M. F. Crommie, R. A. Segalman, S. G. Louie and F. Wang, *Nature*, 2011, **471**, 617–620.
35 N. Mattiucci, R. Trimm, G. D'Aguanno, N. Aközbek and M. J. Bloemer, *Appl. Phys. Lett.*, 2012, **101**, 141115.
36 A. Alù, G. D'Aguanno, N. Mattiucci and M. J. Bloemer, *Phys. Rev. Lett.*, 2011, **106**, 123902.
37 C. Argyropoulos, G. D'Aguanno, N. Mattiucci, N. Akozbek, M. J. Bloemer and A. Alù, *Phys. Rev. B: Condens. Matter Mater. Phys.*, 2012, **85**, 024304.
38 J. Chen, M. Badioli, P. Alonso-González, S. Thongrattanasiri, F. Huth, J. Osmond, M. Spasenović, A. Centeno, A. Pesquera, P. Godignon, A. Z. Elorza,

N. Camara, F. J. García de Abajo, R. Hillenbrand and F. H. L. Koppens, *Nature*, 2012, **487**, 77–81.
39 Z. Fei, A. S. Rodin, G. O. Andreev, W. Bao, A. S. McLeod, M. Wagner, L. M. Zhang, Z. Zhao, G. Dominguez, M. Thiemens, M. M. Fogler, A. H. Castro-Neto, C. N. Lau, F. Keilmann and D. N. Basov, *Nature*, 2012, **487**, 82–85.
40 H. Meng, L. Wang, G. Liu, X. Xue, Q. Lin and X. Zhai, *Appl. Opt.*, 2017, **56**, 6022–6027.